Axial force evaluation in permanent magnet thrust bearings subject to demagnetization and temperature effects

Maxence Van Beneden, Virginie Kluyskens, Bruno Dehez

Center for Research in Mechatronics (CEREM), Institute of Mechanics, Materials and Civil Engineering (IMMC),
Université catholique de Louvain (UCL), Louvain-la-Neuve 1348, Belgium
maxence.vanbeneden@uclouvain.be

***Abstract*—This article presents a 2D axisymmetric finite element model allowing to evaluate the axial force developed by a permanent magnet thrust bearings, including demagnetization and temperature effects. For this purpose, a linearized B-H curve is included in the model, with coefficients depending on the temperature. The axial force evaluation, as a function of the operating temperature is validated experimentally on a test bench. Finally, based on this model, the performance of thrust bearings using either SmCo or NdFeB are compared.**

I. INTRODUCTION

Nowadays, permanent magnets (PM) are increasingly used in applications e.g. maglev, motors, eddy current brakes and magnetic bearings [1]. Thanks to the recent development of rare-earth magnet [2], the PM properties are improved with a greater:

- maximum energy product,
- ability to withstand demagnetization,
- temperature stability.

Two main categories of rare-earth PM are commonly available on the market: the samarium cobalt *SmCo* and the neodymium iron bore *NdFeB*. The former present lower variations of their remanence and coercivity with an increase of temperature and the latter reach higher values of maximum energy product and higher coercitive fields.

Despite progress/improvements made on the rare earth permanent magnet properties, PM materials are still subject to a risk of demagnetization. This risk is notably due to (i) external applied magnetic field and (ii) to PM properties including coercivity and temperature dependence. This means that the risk of demagnetization is strongly dependent on the PM material but also on the equivalent magnetic circuit. From permanent magnet manufacturers, few information is given regarding the PM properties apart from a maximal operating temperature. This maximal temperature is given as an advice for basic design, but this information is not sufficient. For instance, in [3] and [4], authors work on modeling PM machine and take into account the demagnetization and the temperature effect. They show that these effects can impact results and in some cases need to be considered for a good prediction of PM devices.

To the author's knowledge, there is no publication about the demagnetization or temperature effect on PM bearings. PM bearings are made of PM magnets opposing or attracting to each other. Efficient PM bearings, in terms of PM volume, are made of axial or radial stacks of pairs of PM rings axially or radially polarized [5]. One stack is linked to the stator and the other stack to the rotor. Their aim is to either generate axial/radial force to compensate static effort, and/or develop axial/radial stiffness. In the literature [6–7], authors use some models to evaluate force and stiffness but do not take into consideration demagnetization or temperature effect. Therefore, these effects are not considered for the sizing, the optimization or the comparison of PM bearings and no study is done on the impact of the PM properties.

This paper describes the finite element model (FEM) used to evaluate the axial force generated by PM thrust bearings (PMTB). The demagnetization and the temperature effect are included in this model. The results of the FEM are validated experimentally. Based on this FEM, the performances of PMTB made of SmCo and NdFeB are compared.

In Section 2, the demagnetization model is presented and the temperature effect is added. The FEM is introduced in Section 3 and illustrated on a study case. It is validated through experiments in section 4. Finally in section 5, the results are discussed and a comparison of the samarium cobalt and the neodymium iron bore PM is made.

II. DEMAGNETIZATION MODELLING

This section describes the demagnetization curve used in the finite element model. It is divided into two subsections. First, the reversible and irreversible demagnetization curves are given. Secondly, the temperature effect is described.

A. Reversible and irreversible demagnetization

PM materials are usually characterized by their polarization curve J-H or their magnetic flux density curve B-H, linking respectively the evolution of the polarization $\vec{J}$ and

the magnetic flux density $\vec{B}$ to the magnetic field $\vec{H}$. In [3], authors model the polarization $\vec{J}$ in PM as solely due to the magnetic field parallel to the polarization. In [8], they prove that the perpendicular field need, in some cases, to be considered. However most of authors [9], [10] neglect the influence of the perpendicular field, leading to:

$$\begin{aligned} \vec{B}_{\parallel} &= \mu_0 \mu_r \vec{H}_{\parallel} + \vec{J}\left(\vec{H}_{\parallel}\right) \\ \vec{B}_{\perp} &= \mu_0 \mu_r \vec{H}_{\perp} \end{aligned} \tag{1}$$

with μ_0 the vacuum permeability and μ_r the relative permeability of the PM.

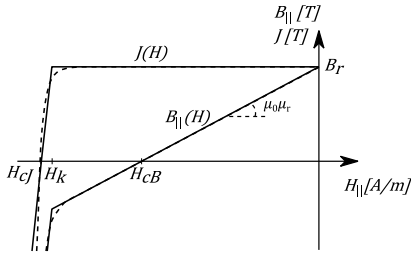

Figure 1. B-H and J-H curve of PM material. B_r: the remanence, H_{cJ}: the coercivity of the polarization $\vec{J}$, H_k the knee point of the demagnetization and H_{cB} the coerivity of the magnetic flux density. Continuous line: piecewise linear approximated curve, broken line: actual curve.

Figure 1 shows the evolution of the J-H and B-H curves. They are characterized by some specific points, i.e. the remanence B_r, the coercivity of the polarization H_{cJ} and the coercivity of the magnetic flux density H_{cB}. In addition, they can be divided in two domains from either side of the knee point H_k:

- a domain of reversible demagnetization, in which the magnetic flux density decreases slowly;
- a domain of irreversible demagnetization, in which the magnetic flux density decrease drastically.

Different approximations of the J-H curve can be found in the literature [9], [10]. In this paper, a piecewise linear curve is used. The linear interpolation of the polarization $\vec{J}$ is done by:

$$\left|\vec{J}\right| = \begin{cases} B_r & \text{for } \left|\vec{H}_{\parallel}\right| \geq H_k \\ \frac{B_r}{H_{cJ}-H_k}\left(H_{cJ} - \left|\vec{H}_{\parallel}\right|\right) & \text{for } H_k \leq \left|\vec{H}_{\parallel}\right| \leq 2H_{cJ} - H_k \\ -B_r & \text{for } \left|\vec{H}_{\parallel}\right| \leq 2H_{cJ} - H_k \end{cases} \tag{2}$$

No hysteresis model is implemented. Consequently, the recoil curve cannot be estimated.

B. Temperature effect

The remanence B_r and coercivity H_{cJ-B} of PM decrease with an increasing temperature as shown in Fig. 2. In [11], authors show that both quantities are dependent on temperature and can be represented using a second order polynomial equation. From PM manufacturer [12], only the linear coefficient is given and expressed in $[\%/K]$:

- the temperature coefficient of the remanence α_{B_r};
- the temperature coefficient of the coercivity α_H, identical for both the coercivity of the polarization and the coercivity of the magnetic flux density.

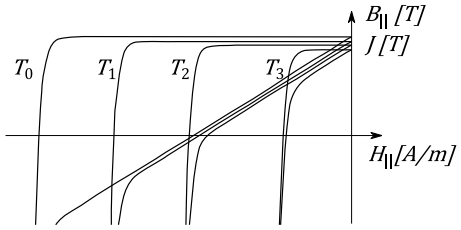

Figure 2. BH and BJ curve of PM material subect to different temperatures: $T_0 < T_1 < T_2 < T_3$.

Finally the evolution with the temperature of the remanence and coercivity can be expressed respectively by:

$$\begin{aligned} B_r &= B_{r,20°C}\left(1 - \alpha_{B_r}\frac{(T-20°C)}{100}\right) \\ H_k &= H_{k,20°C}\left(1 - \alpha_H\frac{(T-20°C)}{100}\right) \\ H_{cJ} &= H_{cJ,20°C}\left(1 - \alpha_H\frac{(T-20°C)}{100}\right) \end{aligned} \tag{3}$$

III. FINITE ELEMENT MODEL

In order to evaluate the impact of the demagnetization and the temperature on the performance of a PM bearing, constitutive equations (1), (2) and (3) are implemented into a FE software. In addition, the model also considers:

- an isotropic relative permeability for all the materials,
- a linear ferromagnetic material.

To reduce the computation time, the model benefits from the axial and plane symmetries of the system.

Practically, the FE model is implemented in COMSOL, the magnetic field is solved by the scalar magnetic potential and the axial force is evaluated by integration of the Maxwell stress tensor.

TABLE I. DIMENSIONS AND PROPERTIES OF THE PM RINGS (N38H GRADE)

	Parameter	Value
D	Outer PM diameter	50 mm
d	Inner PM diameter	30 mm
h	PM height	5 mm
B_r	Remanence	1.24 T
$\mu_{r_{PM}}$	PM relative permeability	1.0588
H_k	Coercivity: knee point	1380 kA/m
H_{cJ}	Polarization coercivity	1420 kA/m
α_{B_r}	Temperature coefficient of remanence	0.115 $\%/K$
α_H	Temperature coefficient of coercivity	0.58 $\%/K$
T_{max}	Maximal working temperature	120 °C

To illustrate the model, an application case is presented with two opposed PM rings with axial polarization mounted with a soft magnetic materials on the back. The dimensions of the iron core are given in Fig. 3.a and the dimensions and properties of the PM rings are in Table I. Figure 3.b shows the FE model with its symmetries, the contour used to perform the Maxwell stress integration, and the mesh for an airgap of 2.6 mm. The relative permeability of iron is supposed to be isotropic and equal to 5000.

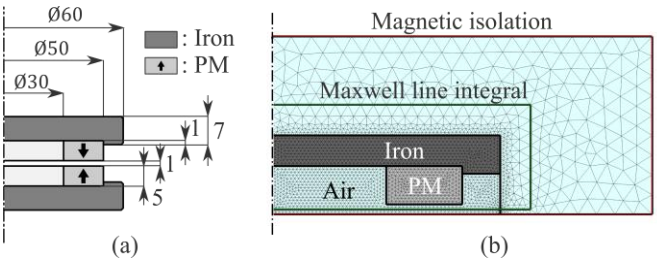

Figure 3. (a) Dimensions of iron core and PM rings and (b) FE model and mesh for an airgap of $g = 2.6\ mm$.

The axial force F_z is evaluated for different values of temperature and airgap thickness:

$$F_{z,ij} = f(T_i, g_j) \tag{4}$$

with T_i the temperature ranging from 20°C to 140°C in steps of 5°C and g_j the airgap form 0.2 mm to 3.8 mm in steps of 0.1 mm. The results are given in Fig. 4 for four particular airgap values.

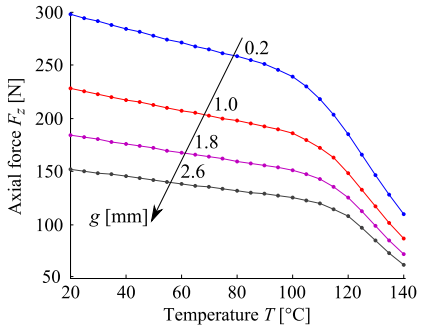

Figure 4. Evolution of the axial force with the temperature from 20°C to 140 °C by step of 5°C for different air gap g

Based on these values of the axial force $F_{z,ij}$, a linear interpolation is made to deduce from a temperature T' and an axial force F_z' the corresponding airgap g':

$$g' = f'(T', F_z') \tag{5}$$

This function is used in section VI to compare the FEM with the experimental results.

IV. Experimental Test Bench

To validate the FE model, a test bench shown on Fig. 5 has been realized. The detailed cross-section view of the system is shown in Fig. 6. The test bench allows to observe the evolution of the distance between two identical PM rings with axial but opposite polarization with regards to the axial force F_z and the temperature T. Each ring is mounted with a soft magnetic materials on the back. One ring is fixed on the static part and the other on a shaft radially guided by air bearings. The airgap thickness is measured by a non-contact capacitive displacement sensor. The axial force remains constant for each test by applying different masses. The complete test bench is placed in a temperature controlled oven.

Figure 5. On the left side, the test bench and on the right side the PM rings.

The dimensions and properties of the PM rings are given in Table I. The properties correspond to a N38H grade material (NdFeB). A centering diameter Ø50 of 1mm deep is machined on the rotor and stator iron core.

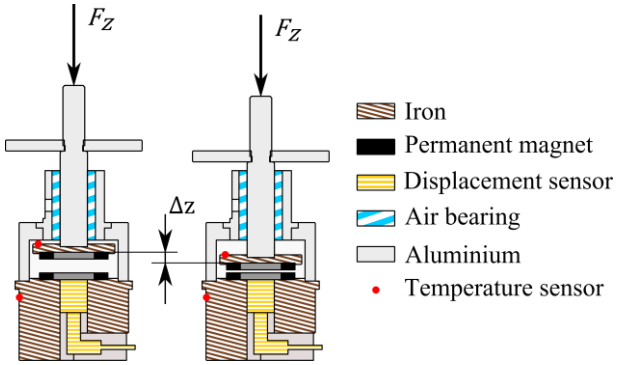

Figure 6. Schematic drawing of the bench test used to evaluate the axial distance z between the 2 PM rings. The axial force F_z is constant and is imposed by different masses. The bench test is placed in a oven and the temperatures vary form 20°C to 130 °C.

The accuracy strongly depends on the precision of the measured PM temperature. Two problems have to be solved. First, due to temperature gradient and pressurized air injected by the air bearing, the temperature is not uniform and therefore is not the same for the two PM rings. Secondly, this temperature cannot be directly taken on the PM rings. Different temperature sensors (thermocouple) are placed close to the rotor and stator PM rings on the iron core as shown in Fig. 6. The oven temperature is slowly increased to maintain the maximum temperature difference between both sensors around 5°C. For the example, the measured temperature during one cycle is given in Fig. 7.a and the difference between the two sensors is given in Fig. 7.b. Moreover the air flow in the air bearing is very low and has a little impact on the PM

temperature. The PM temperature is supposed to be equal to the temperature of the rotor sensor.

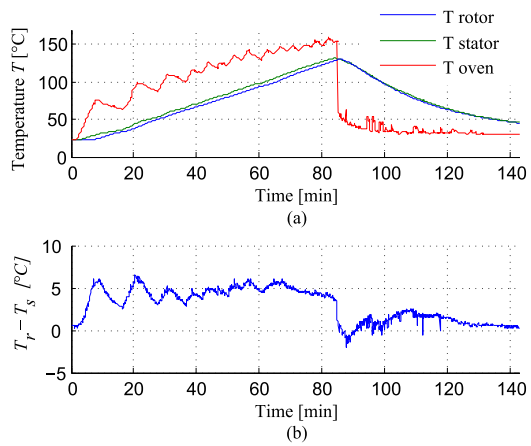

Figure 7. (a): Measured temperature inside the oven, on the rotor and stator iron core. (b): Difference between the rotor and stator measured temperature.

V. VALIDATION AND DISCUSSION

In this section, the results from the FE model are compared with the experimental results. Then some discussions about the demagnetization aspect are given and a comparison between thrust bearings made of different PM material is provided.

A. Validation

Figure 8 compares the FE results taking into account the demagnetization effects as described by (2) and the experimental results at room temperature (20°C). It shows the evolution of the axial force with the airgap. As expected, the axial force decreases when the airgap thickness increases. Results show a very good agreement between FE results and experiments.

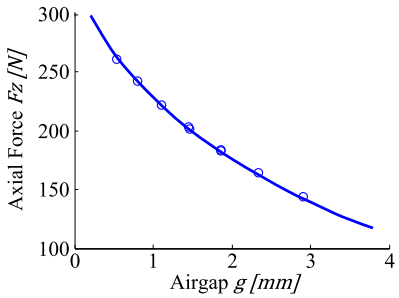

Figure 8. Evolution of the axial force in fuction of the airgap at room temperature of 20°C. Solid line: FE results. Points: experimental results.

In Fig. 9, The FE results (5) are compared with experimental results. The evolution of the airgap thickness with the temperature is shown, for an imposed constant axial force on the PM rings. Each curve in Fig. 9, illustrating the behavior for different imposed axial loads, has been measured with a new unaltered couple of identical PM rings. A good agreement is found except at the knee point where experiments show smaller airgaps than the FE results. This difference is a priori due to the model of the demagnetization curve (2). The latter is done by piecewise linear interpolation as explained in section 2. This interpolation overestimates the value of the remanence in the knee point region leading in an overestimated axial force in the model, which means a higher airgap. Nevertheless, the FE results are good enough to predict the demagnetization behavior.

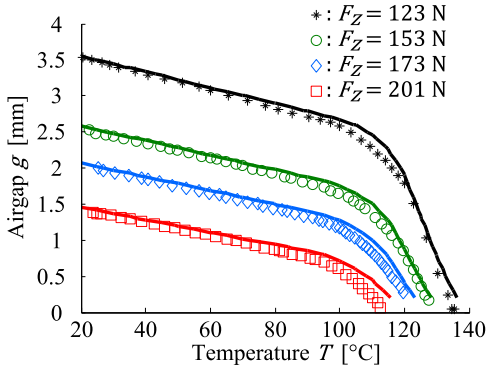

Figure 9. FE (solid line) and experimental (points) results of the evolution of the airgap thickness g with an inceasing temperature T for different constant axial forces F_z.

Finally, an experiment is performed to show the recovery curve after different temperature cycles while keeping the same couple of PM rings. The results are presented in Fig. 10 and show the evolution of the airgap thickness g with the temperature T for a constant axial force of $F_z = 123N$. A first cycle is done in the reversible region where the maximal temperature is $T = 90°C$. A second cycle reaches a temperature of $T = 120°C$ and the recovery curve is slightly lower than the initial curve. Cycles 3 and 4 reach respectively a temperature of 132°C and 136°C.

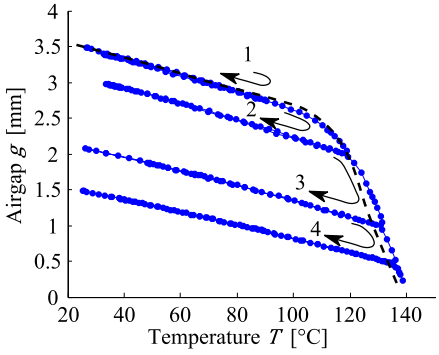

Figure 10. Evolution of the airgap thickness with the temperature for a constant axial force $F_z = 123\ N$. The temperature is increased and decreased in 4 different cycles. The cycle 1 stays in the reversible demagnetization region ($T < 90°C$). Cycles 2, 3 and 4 are subject to irreversible demagnetization. In dashed line, FE results of Fig. 9.

B. Discussion and comparison

Based on the FE model, two PM materials are compared: the samarium cobalt *SmCo* and the neodymium iron bore *NdFeB*. In table II, the properties of two particular PM material used for this comparison are given: YXG32 (*SmCo)* and N38H (*NdFeB)*. The dimensions of PM rings and the conditions of

simulation are exactly the same than in previous sections (see Fig. 3).

TABLE II. PROPERTIES OF TWO PM MATERIAL: THE SAMARIUM COBALT AND THE NEODYMIUM IRON BORE

	Parameters	*SmCo* YXG32	*NdFeB* N38H
B_r	Remanence	1.11 T	1.24 T
$\mu_{r_{PM}}$	PM relative permeability	1.0553	1.0588
H_k	Coercivity: knee point	910 kA/m	1380 kA/m
H_{cJ}	Polarization coercivity	1700 kA/m	1420 kA/m
H_k/H_{cJ}		54 %	97 %
α_{B_r}	Temperature coefficient of remanence	0.035 %/K	0.115 %/K
α_H	Temperature coefficient of coercivity	0.2 %/K	0.58 %/K
T_{max}	Maximal working temperature	300 °C	120 °C

In Fig. 11, the FE results for both materials show the evolution of the axial force with the temperature for four different values of constant airgap, as shown by (4). The solid lines curves represent the predicted axial force when considering irreversible demagnetization and in dashed line, when considering the demagnetization curves without the irreversible effects. The temperature T_{irrev} represents the temperature where the two curves diverge, and its value is indicated on the figure for each airgap. At this point, the maximal value of the magnetic field of some local regions inside the PM and parallel to the polarization reaches the value of the knee point coercivity: $\max|H_{\parallel}| = H_k$. If the temperature is higher than T_{irrev}, the PM material is subjected to irreversible demagnetization. The values of T_{irrev} illustrated in Fig. 11 are also summarized for different airgap thicknesses and for the both PM materials in Table III. The temperature corresponding to a null axial force is 500°C for *SmCo* and 180°C for *NdFeB* and is the same for all airgap thickness. Some analyses are done on this figure.

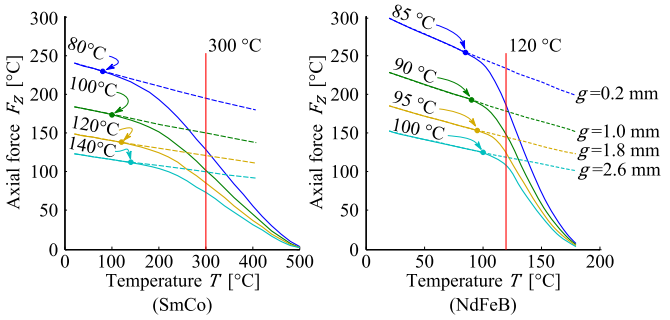

Figure 11. Evolution of the axial force with the temperature for 4 different airgap thicknesses $g = [0.2\ ;\ 1.0\ ;\ 1.8\ ;\ 2.6]\ mm$. On the left side, the YXG32 samarium cobalt and on the right side the N38H neodymium iron bore. The maximal recommended working temperature is 300°C for *SmCo* and 120°C for *NdFeB*. In dashed line: curve without considering irrversible demagnetization.

First, the parameters that influence the temperature T_{irrev}, are studied. This temperature T_{irrev} where the PM material become irreversibly demagnetized, depends on:

(i) an external applied magnetic field $H_{\parallel}$.
(ii) the PM properties.

The increase of the external magnetic field $H_{\parallel}$ happens when the airgap thickness decreases. In Table III, we observed that for *SmCo*, the temperature T_{irrev} is more variable with the airgap thickness than for *NdFeB*. The reason is that *SmCo* have poor resistance to demagnetization in comparison to the *NdFeB*:

– $H_{k,20°C}^{SmCo} = 910\ kA/m$,
– $H_{k,20°C}^{NdFeB} = 1380\ kA/m$

with $H_{k,20°C}$ the coercivity knee point at $20°C$. This means that even at low temperature, *SmCo* have a risk of demagnetization if the magnetic field $H_{\parallel}$ is significant. In contrast, *NdFeB* resists to irreversible demagnetization but not to temperature effect. Thus, the range of temperature for T_{irrev} is small.

Secondly, the temperature T_{irrev} is compared with the maximum working temperature T_{max} suggests by the PM manufacturer. As observed in Fig. 11, the temperature from manufacturers T_{max} (vertical red line) does not correspond to the temperature T_{irrev} (points indicated with the arrows). The temperature T_{irrev} is even more restrictive for the application cases presented here than the maximal temperature T_{max}. Consequently, a model where both reversible and irreversible effects, is needed to safely design PM bearings for applications with high or variable operating temperature.

TABLE III. MAXIMAL TEMPERATURE T_{irrev} BEFORE IRREVERSIBLE DEMAGNETIZATION FOR DIFFERENT AIRGAP THICKNESS AND FOR NEODYMIUM IRON BORON AND SAMARIUM COBALT MAGNET

Airgap thickness g	Temperature before irreversible demagnetization T_{irrev}	
	SmCo (YXG32)	*NdFeB* (N38H)
0.2 mm	80 °C	85 °C
1.0 mm	100 °C	90 °C
1.8 mm	120 °C	95 °C
2.6 mm	140 °C	100 °C

Thirdly, the comparison between the *SmCo* and *NdFeB* materials is done in the two regions: in the reversible regions ($T \leq T_{irrev}$) and in the irreversible region ($T > T_{irrev}$).
For the reversible region, the temperature has less impact on the *SmCo* material than on the *NdFeB*. Indeed, the axial force depends on the square of the polarization [7], with $J_{\parallel} = B_r$ leading to:

$$F_{z,T} = F_{z,20°C}\left(1 - \alpha_{B_r}\frac{T-20°C}{100}\right)^2 \approx F_{z,20°C}\left(1 - 2\alpha_{B_r}\frac{T-20°C}{100}\right) \quad (6)$$

The temperature coefficient of remanence α_{B_r} for the *SmCo* is approximatively 3 times smaller than the coefficient of the *NdFeB*. Consequently, the influence of the temperature on the force is approximatively 3 times smaller for *SmCo* than for *NdFeB*.

For the irreversible region, we observe that *SmCo* decreases slowly with the temperature in comparison to the *NdFeB*. Actually, the range of temperature during the irreversible demagnetization is from 80 – 140°C to 500°C for *SmCo* and from 85 – 100°C to 180°C for *NdFeB*. This is explained by the ratio H_k/H_{cJ} and the temperature coefficient of coercivity α_H. As shown in Table II, *NdFeB* have higher value of H_k/H_{cJ} than *SmCo*. This means that the irreversible demagnetization is abrupt inside the *NdFeB*. Moreover, they have bad resistance to irreversible demagnetization with the temperature. The coefficient α_H is approximatively 3 times greater for *NdFeB* than for *SmCo*. Consequently, the risk of abrupt irreversible demagnetization is important for the $NdFeB$ magnet and some care has to be taken when this kind of PM are used inside applications presenting peak of temperatures. In opposite, even if *SmCo* are subject to irreversible effect leading in a diminution of the performance, the risk of abrupt demagnetization is lower.

Finally, to illustrate the demagnetization process, Fig. 12 shows the local polarization $|\vec{J}|$ obtained from the FEM for both material with a constant airgap thickness of $g = 1mm$, while increasing the ambient temperature. In the regions subjected to reversible demagnetization, represented by light grey color, the polarization is uniform and the axial force temperature dependence respects (6). The PM are also subject to local irreversible demagnetization, which is represented in graduated color. For this kind of PM thrust bearing, with only one couple of PM rings facing each other and presenting a back iron yoke, the irreversible demagnetization happens starting from the center of the PM, on the airgap side. The effect of the back iron yoke is also visible on the external side of the PM, next to the 1 mm deep centering diameter. This corner is the last one to be subject to irreversible demagnetization. Similarly, to previous observations, it can be observed that, for *SmCo* PM thrust bearing, the temperature range is much larger than for *NdFeB* PM thrust bearing.

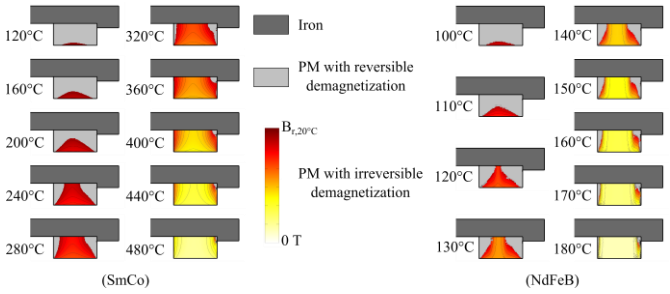

Figure 12. Amplitude of the local polarization $|\vec{J}|$ with reversible and irreversible demagnetization zone for different temperature T and a constant airgap tickness $g = 1\ mm$. On the left side for *SmCo* (YXG32) and on the right side *NdFeB* (N338H) material.

VI. Conclusion

From permanent magnet machine literature, a finite element model is adapted to permanent magnet thrust bearings. This model takes into account the reversible and irreversible demagnetization effect together with temperature effect. The model is experimentally validated thanks to a test bench allowing a measure of the airgap thickness evolution with the temperature for different axial forces. Based on this model, simple permanent magnet thrust bearings made of samarium cobalt or neodymium iron boron magnet are compared. The comparison confirms the classical distinction between both materials:

- *SmCo* are more stable with temperature,
- *NdFeB* have greater energy density and withstand better demagnetization.

However, this paper shows that in applications where temperature or demagnetization effect is critical, sizing PM bearings need a more complete model, such as the one presented in this article.

A last comment can be done. The values presented here are only valid for these application cases. Indeed, these results are strongly dependent of the airgap thickness, PM dimensions, PM properties and so on. Then with another set of parameters, the results could be very different. However, the observations made on the comparison between PM materials remain valid in a more general way and the conclusion on the need of prediction of the demagnetization ant temperature effect stay correct.

Acknowledgement

The authors would like to acknowledge the support of the "Walloon Region" in carrying out the research work.

References

[1] M. T. Thompson, "Practical issues in the use of NdFeB permanent magnets in maglev, motors, bearings, and eddy current brakes," *Proceedings of the IEEE*, vol. 97, no 11, p. 1758–1767, 2009.

[2] Magnets Rare-Earth Permanent VACODYM VACOMAX, "Company Information Booklet PD-002", Ed. 2015, Vacuumschmeltze GmbH & Co. KG (VAC)

[3] S. Sjökvist et S. Eriksson, "Study of demagnetization risk for a 12 kW direct driven permanent magnet synchronous generator for wind power," *Energy Science & Engineering*, vol. 1, nº 3, p. 128–134, 2013.

[4] S. Ruoho, J. Kolehmainen, J. Ikäheimo, and A. Arkkio, "Interdependence of demagnetization, loading, and temperature rise in a permanent-magnet synchronous motor," *IEEE Trans. Magn*, vol. 46, nº 3, p. 949–953, 2010.

[5] M. Van Beneden, V. Kluyskens, et B. Dehez, "Optimal sizing and comparison of permanent magnet thrust bearings," *IEEE Trans. Magn.*, vol. 53, nº 2, p. 1–10, 2017.

[6] G. Jungmayr, E. Marth, W. Amrhein, H.-J. Berroth, et F. Jeske, "Analytical stiffness calculation for permanent magnetic bearings with soft magnetic materials," *IEEE Trans. Magn.*, vol. 50, nº 8, p. 1–8, 2014.

[7] J.-P. Yonnet, "Permanent magnet bearings and couplings," *IEEE Trans. Magn.*, vol. 17, nº 1, p. 1169–1173, 1981.

[8] S. Ruoho and A. Arkkio, "Partial demagnetization of permanent magnets in electrical machines caused by an inclined field," *IEEE Trans. Magn*, vol. 44, nº 7, p. 1773–1778, 2008.

[9] S. Ruoho, E. Dlala, and A. Arkkio, "Comparison of demagnetization models for finite-element analysis of permanent-magnet synchronous machines," *IEEE Trans. Magn*, vol. 43, nº 11, p. 3964–3968, 2007.

[10] P. Zhou, D. Lin, Y. Xiao, N. Lambert, and M. A. Rahman, "Temperature-dependent demagnetization model of permanent magnets for finite element analysis," *IEEE Trans. Magn*, vol. 48, nº 2, p. 1031–1034, 2012.

[11] M.-D. Calin and E. Helerea, "Temperature influence on magnetic characteristics of NdFeB permanent magnets," in *Advanced Topics in Electrical Engineering (ATEE), 2011 7th International Symposium on*, 2011, p. 1–6.

[12] Permanent magnet manufacturer – "HKCM Engineering e.K." Ottestr.20, 24340 Eckernförde, Germany